

Cosmic Magnetic Fields: Observations and Prospects

Rainer Beck

Max-Planck-Institut für Radioastronomie, Auf dem Hügel 69, 53121 Bonn, Germany

Abstract. Synchrotron emission, its polarization and its Faraday rotation at radio frequencies of 0.2–10 GHz are powerful tools to study the strength and structure of cosmic magnetic fields. Unpolarized emission traces turbulent fields which are strongest in galactic spiral arms and bars (20–30 μG) and in central starburst regions (50–100 μG). Such fields are dynamically important, e.g. they can drive gas inflows in central regions. Polarized emission traces ordered fields which can be regular (uni-directional) or anisotropic random (generated from isotropic random fields by compression or shear). Ordered fields with spiral patterns exist in grand-design, barred and flocculent galaxies, and in central regions of starburst galaxies. The strongest ordered (mostly regular) fields of 10–15 μG strength are generally found in galactic interarm regions and follow the orientation of adjacent gas spiral arms. Faraday rotation measures (RM) of the diffuse polarized radio emission from the disks of several spiral galaxies reveal large-scale patterns, which are signatures of regular fields probably generated by a mean-field dynamo. Ordered fields in interacting galaxies have asymmetric distributions and are an excellent tracer of past interactions between galaxies or with the intergalactic medium. Ordered magnetic fields are also observed in radio halos around edge-on galaxies, out to large distances from the plane, with X-shaped patterns. – The strength of the total magnetic field in our Milky Way is about 6 μG near the solar radius, but several mG in dense clouds, pulsar wind nebulae, and filaments near the Galactic Center. Diffuse polarized radio emission and Faraday rotation data from pulsars and background sources show spiral fields with large-scale reversals, but the overall field structure in our Galaxy is still under debate. – Diffuse radio emission from the halos of galaxy clusters is mostly unpolarized because intracluster magnetic fields are turbulent, while cluster “relics”, probably shock fronts by cluster mergers, can have degrees of polarization of up to 60% and extents of up to 2 Mpc. The IGM magnetic field strength is $\geq 3 \cdot 10^{-16}$ G with a filling factor of at least 60%, derived from the combination of data from the HESS and FERMI telescopes. – Polarization observations with the forthcoming large radio telescopes will open a new era in the observation of cosmic magnetic fields and will help to understand their origin. At low frequencies, LOFAR (10–250 MHz) will allow us to map the structure of weak magnetic fields in the outer regions and halos of galaxies and galaxy clusters. Small Faraday rotation measures can also be best measured at low frequencies. Polarization at higher frequencies (1–10 GHz), as observed with the EVLA, MeerKAT, APERTIF and the SKA, will trace magnetic fields in the disks and central regions of nearby galaxies in unprecedented detail. The SKA pulsar survey will find many new pulsars; their RMs will map the Milky Way’s magnetic field with high precision. All-sky surveys of Faraday rotation measures towards a dense grid of polarized background sources with the SKA and its precursor telescope ASKAP are dedicated to measure magnetic fields in distant intervening galaxies, galaxy clusters and intergalactic filaments, and will be used to model the overall structure and strength of the magnetic field in the Milky Way. With the SKA, ordered fields in distant galaxies and cluster relics can be measured to redshifts of $z \simeq 0.5$, turbulent fields in starburst galaxies or cluster halos to $z \simeq 3$ and regular fields in intervening galaxies towards QSOs to $z \simeq 5$.

Keywords: ISM: magnetic fields – Galaxy: spiral structure – galaxies: clusters: intracluster medium – galaxies: evolution – galaxies: halos – galaxies: interactions – galaxies: ISM – galaxies: magnetic fields – galaxies: spiral – intergalactic medium – radio continuum: galaxies

PACS: 98.35.Eg, 98.52.Nr, 98.52.Sw, 98.56.Ne, 98.58.Ay, 98.62.Ai, 98.62.En, 98.62.Gq, 98.62.Hr, 98.65.Hb

INTRODUCTION

Observations and modeling of cosmic magnetic fields revealed that they are a major agent of the interstellar medium (ISM) and the intracluster medium (ICM). They contribute significantly to the total pressure which balances the gas disk of galaxies against gravitation. They affect the dynamics of the turbulent ISM [37] and the gas flows in spiral arms [57]. The shock strength in spiral density waves is decreased and structure formation is reduced in the presence of strong fields [39]. The interstellar fields are closely connected to gas clouds. Magnetic fields stabilize gas clouds and reduce the star-formation efficiency to the observed low values [108, 140]. On the other hand, magnetic fields are essential for the onset of star formation as they enable the removal of angular momentum from the protostellar cloud via ambipolar diffusion [72]. *MHD turbulence* distributes energy from supernova explosions within the ISM [127] and drives field amplification and ordering via a *dynamo* (see below).

Magnetic fields also control the density and distribution of cosmic rays in the ISM. Cosmic rays accelerated in supernova remnants can provide the pressure to drive a *galactic outflow* and buoyant loops of magnetic fields via the *Parker instability* [64]. Parker loops can in turn drive a dynamo [65]. Outflows from starburst galaxies in the early Universe may have magnetized the intergalactic medium [88]. Understanding the interaction between the gas and the magnetic field is a key to understand the physics of galaxy disks and halos and the evolution of galaxies.

The detection of ultrahigh-energy cosmic rays (UHECRs) with the AUGER observatory and the anisotropic distribution of their arrival directions [1] calls for a proper model of particle propagation. As UHECR particles are deflected by large-scale regular fields and scattered by turbulent fields, the structure and the extent of the fields in the disk and halo of the Milky Way need to be known, but the present data do not allow safe conclusions [98, 103].

Some fraction of massive galaxy clusters have radio halos which require the generation of intracluster magnetic fields and the acceleration of cosmic ray particles. The magnetic fields can affect thermal conduction [5, 105] and hence the dynamics and evolution of the intracluster medium.

In spite of our increasing knowledge, many important questions, especially the origin and evolution of magnetic fields, their first occurrence in young galaxies and galaxy clusters, or the strength and structure of intergalactic fields remained unanswered.

ORIGIN OF MAGNETIC FIELDS

Seed fields may be “primordial”, generated during a phase transition in the early Universe [25, 146], or originate from the time of cosmological structure formation by the Weibel instability [94], or from injection by the first stars or jets generated by the first black holes [110], or from the Biermann mechanism in the first supernova remnants [66].

The most promising mechanism to sustain magnetic fields in the interstellar medium of galaxies is the dynamo [10]. The small-scale or *fluctuation dynamo* [19] does not need general rotation, only turbulent gas motions. It amplifies weak seed fields to the energy density level of turbulence. A small-scale dynamo in protogalaxies may have amplified

seed fields to several μG strength (the energy level of turbulence) within less than 10^8 yr [117]. To explain the generation of large-scale fields in galaxies, the mean-field dynamo has been developed. It is based on turbulence, differential rotation and helical gas flows (α -effect), driven by supernova explosions [44, 61]. The mean-field dynamo in galaxy disks predicts that within a few 10^9 yr large-scale regular fields are generated from μG turbulent fields [3], forming spiral patterns (*modes*) with different azimuthal symmetries in the disk and vertical symmetries in the halo (see below). Global numerical models of galaxies [55, 65] confirm the basic results of the mean-field approximation.

The mean-field dynamo generates large-scale helicity with a non-zero mean in each hemisphere. As total helicity is a conserved quantity, the dynamo is quenched by the small-scale fields with opposite helicity unless these are removed from the system [121]. Outflows are probably essential for effective mean-field dynamo action.

In the intracluster medium, the seed fields ejected by galactic jets or winds are probably amplified by a small-scale dynamo driven by turbulent gas motions [17, 128].

TOOLS TO STUDY MAGNETIC FIELDS

Magnetic fields need illumination to be detectable. *Polarized emission* at optical, infrared, submillimeter and radio wavelengths holds the clue to measure magnetic fields in galaxies. Optical linear polarization is a result of extinction by elongated dust grains in the line of sight which are aligned in the interstellar magnetic field (the *Davis-Greenstein effect*). The E-vector runs parallel to the field. However, light can also be polarized by scattering, a process unrelated to magnetic fields and hence a contamination that is difficult to subtract from the diffuse polarized emission from galaxies, e.g. in M 51 [116]. Optical polarization data of about 5500 selected stars in the Milky Way yielded the orientation of the large-scale magnetic field near the sun [50]. Together with measurements of stellar distances, a 3-D analysis of the magnetic field within about 5 kpc from the sun is possible, but more data are needed.

Linearly polarized emission from elongated dust grains at infrared and submillimeter wavelengths is not affected by polarized scattered light. The B-vector is parallel to the magnetic field. The field structure can be mapped in gas clouds of the Milky Way [133] and in galaxies, e.g. in the halo of M 82 [60].

Most of what we know about interstellar magnetic fields comes through the detection of radio waves. *Zeeman splitting* of radio spectral lines directly measures the field strength in gas clouds of the Milky Way [36] and in starburst galaxies [114]. The intensity of *synchrotron emission* is a measure of the density of cosmic-ray electrons in the relevant energy range and of the strength of the total field component in the sky plane. The assumption of energy equipartition between these two components allows us to calculate the total magnetic field strength from the synchrotron intensity [12].

Linearly polarized synchrotron emission emerges from ordered fields in the sky plane. As polarization “vectors” are ambiguous by 180° , they cannot distinguish *regular (coherent) fields*, defined to have a constant direction within the telescope beam, from *anisotropic fields*, which are generated from turbulent fields by compressing or shearing gas flows and frequently reverse their direction within the telescope beam. Unpolarized synchrotron emission indicates *turbulent (random) fields* which have random directions

in 3-D and have been amplified and tangled by turbulent gas flows.

The intrinsic degree of linear polarization of synchrotron emission is about 75%. The observed degree of polarization is smaller due to the contribution of unpolarized thermal emission, which may dominate in star-forming regions, by *Faraday depolarization* along the line of sight and across the beam [24, 123], and by geometrical depolarization due to variations of the field orientation within the beam.

The polarization vector is rotated in a magnetized thermal plasma by *Faraday rotation*. If Faraday rotation is small (in galaxies typically at wavelengths shorter than a few centimeters), the observed B -vector gives the intrinsic field orientation in the sky plane, so that the magnetic pattern can be mapped directly [6]. As the rotation angle is sensitive to the sign of the field direction, only regular fields give rise to Faraday rotation, while anisotropic and random fields do not. Measurements of the Faraday rotation from multi-wavelength observations allow to determine the strength and direction of the regular field component along the line of sight.

The rotation angle $\Delta\chi$ is proportional to the square of the wavelength λ^2 and the *Faraday depth* (FD), defined as the line-of-sight integral over the product of the plasma density and the strength of the field component along the line of sight. The observable *rotation measure* (RM) is defined as $RM = \Delta\chi / \Delta\lambda^2$. If the rotating region is located in front of the emitting region (*Faraday screen*), $RM = FD$. In case of a region with emission and rotation, $RM \approx FD/2$. Several distinct emitting and rotating regions located along the line of sight generate a spectrum of FD components. In such cases, multi-channel spectro-polarimetric radio data are needed that can be Fourier-transformed into Faraday space, called *RM Synthesis* [21, 52, 68, 69]. If the medium has a simple magnetic structure, its 3-D structure can be determined (*Faraday tomography*).

A *grid of RM measurements of polarized background sources* is another tool to study magnetic field patterns in galaxies [125] and in the intracluster medium [86]. A large number of sources is required to recognize the field patterns, to separate the Galactic foreground contribution and to account for intrinsic RMs of the background sources.

The combination of observations of diffuse polarized emission and RM can be used as a test of *magnetic helicity* [104].

TOTAL FIELDS IN GALAXIES

The typical average *equipartition strength* of the total magnetic field [12] in spiral galaxies is about $10 \mu\text{G}$, assuming energy equipartition between cosmic rays and magnetic fields. Radio-faint galaxies like M 31 (Fig. 1) and M 33 [132], our Milky Way's neighbors, have weaker total magnetic fields (about $6 \mu\text{G}$), while gas-rich spiral galaxies with high star-formation rates, like M 51 and NGC 6946 (Fig. 3), have total field strengths of $20 - 30 \mu\text{G}$ in their spiral arms. The strongest total fields of $50 - 100 \mu\text{G}$ are found in starburst galaxies, like M 82 [77] and the "Antennae" NGC 4038/9 [32], and in nuclear starburst regions, like in the centers of NGC 1097 and other barred galaxies [13].

If energy losses of cosmic-ray electrons are significant, especially in starburst regions or massive spiral arms, the equipartition values are lower limits [12] and are probably underestimated in starburst galaxies by a factor of a few [135]. Field strengths of $0.5 - 18 \text{ mG}$ were detected in starburst galaxies by the Zeeman effect in the OH megamaser

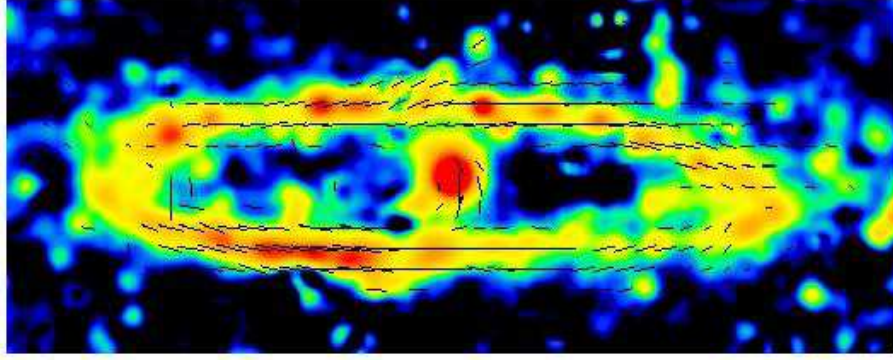


FIGURE 1. Total radio intensity (colors) and B-vectors (corrected for Faraday rotation) in the Andromeda galaxy (M 31), observed at 6 cm with the Effelsberg telescope [15].

emission line at 18 cm [114]. These values refer to highly compressed gas clouds and are not typical for the diffuse interstellar medium.

The relative importance of various competing forces in the interstellar medium are estimated by comparing *energy densities*. The mean energy densities of the total (mostly turbulent) magnetic field and the cosmic rays in NGC 6946 (Fig. 2) and M 33 are $\simeq 10^{-11}$ erg cm $^{-3}$ and $\simeq 10^{-12}$ erg cm $^{-3}$, respectively [7, 132], similar to that of the turbulent gas motions in the star-forming disk, about 10 times larger than that of the ionized gas (*low-beta plasma*). Magnetic fields are dynamically important. The total magnetic energy density may even dominate in the outer galaxy where the equipartition field strength is an underestimate due to energy losses of the cosmic-ray electrons. The energy density of the regular magnetic field decreases even more slowly than that of the total field, possibly because the mean-field dynamo still efficiently operates in the outer disk. Although the star-formation activity is low here, the magneto-rotational instability (MRI) may serve as the source of turbulence required for dynamo action [119].

The integrated luminosity of the total radio continuum emission at centimeter wavelengths (frequencies of a few GHz), which is mostly of nonthermal synchrotron origin, and the far-infrared (FIR) luminosity of star-forming galaxies are tightly correlated. This correlation is one of the tightest correlations known in astronomy. It extends over five orders of magnitude [14] and is valid in starburst galaxies to redshifts of at least 3 [120]. Hence the total radio emission can serve as a tracer of magnetic fields and of star formation out to large distances. The correlation requires that total (mostly turbulent) magnetic fields and star formation are connected, so that the field strength exceeds several 100 μ G in distant galaxies [100]. The tightness needs multiple feedback mechanisms which are not yet understood [91].

The total radio and far-infrared (FIR) or mid-IR (MIR) intensities are also highly correlated within galaxies. The exponent of the correlation in M 51 was found to be different in the central region, spiral arms and interarm regions [41]. The radio-infrared correlation can be presented as a correlation between turbulent field strength and star-formation rate [28]. In contrast, the ordered field is either uncorrelated with the star-formation rate, or anticorrelated in galaxies where the ordered field is strongest in interarm regions with low star formation (Fig. 3). A wavelet cross-correlation analysis

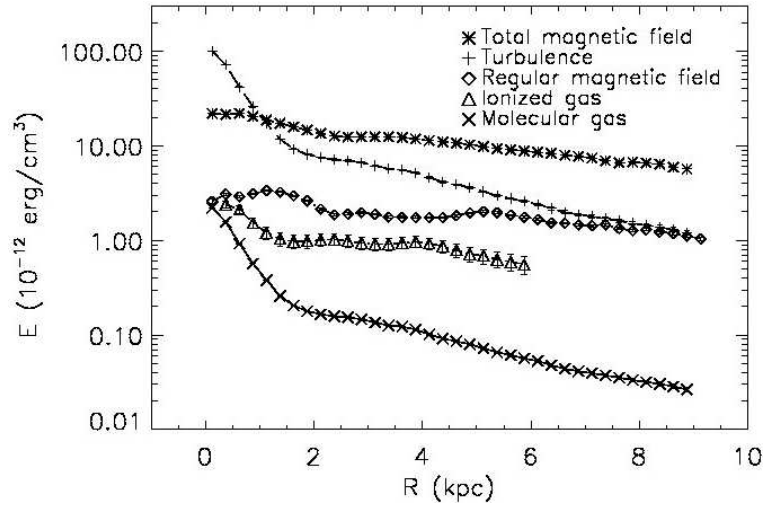


FIGURE 2. Radial variation of the energy densities in NGC 6946: total magnetic field E_B ($B_t^2/8\pi$), regular magnetic field ($B_{reg}^2/8\pi$), turbulent motion of the neutral gas E_{turb} ($0.5\rho_n v_{turb}^2$, where $v_{turb} \approx 7$ km/s), thermal energy of the ionized gas E_{th} ($0.5n_e kT_e$) and thermal energy of the molecular gas E_n ($0.5\rho_n kT_n$), determined from observations of synchrotron and thermal radio continuum and the CO and HI line emissions [7].

for M 33 showed that the radio–FIR correlation holds at all scales down to 1 kpc [131]. The correlation in the Large Magellanic Cloud (LMC) breaks down below scales of about 50 pc [74], probably due to the diffusion of cosmic-ray electrons.

ORDERED MAGNETIC FIELDS IN GALAXIES

Ordered (regular and/or anisotropic) field traced by polarized synchrotron emission form spiral patterns in almost every galaxy [6], even in ring galaxies [29], in flocculent galaxies without massive spiral arms [122] and in the central regions of galaxies and in circum-nuclear gas rings of barred galaxies [13]. Ordered fields are generally strongest (10–15 μG) in the regions *between* the optical spiral arms and oriented parallel to the adjacent spiral arms, in some galaxies forming *magnetic arms*, like in NGC 6946 (Fig. 3 right), with exceptionally high degrees of polarization (up to 50%). These are probably generated by a large-scale dynamo (see below). In galaxies with strong density waves like M 51 [49] enhanced ordered (anisotropic) fields occur at the inner edges of the inner optical arms and in the interarm regions (Fig. 3 left).

The observed *spiral magnetic patterns* with significant pitch angles (in the range $10^\circ - 40^\circ$) indicate a general decoupling between magnetic fields and the gas flow, as predicted by mean-field dynamo action. There is no other model to explain the magnetic spiral patterns in many types of galaxies.

The typical degree of radio polarization within the spiral arms is only a few %; hence the field in the spiral arms must be mostly tangled or randomly oriented within the telescope beam, the width of which corresponds to a few 100 pc. Turbulent fields in spiral arms are probably generated by turbulent gas motions related to star formation

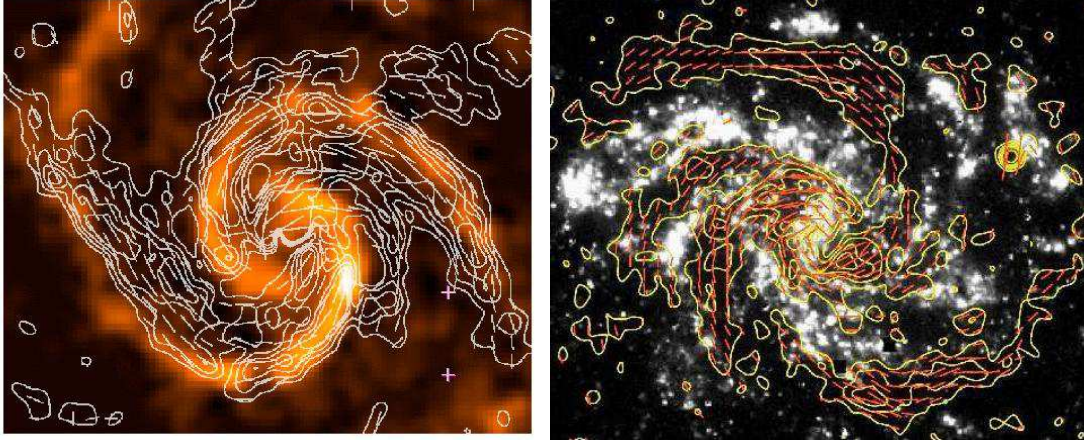


FIGURE 3. **Left:** Polarized radio intensity (contours) and B-vectors in the inner $3' \times 4'$ of M 51, combined from observations at 6 cm wavelength with the VLA and Effelsberg telescopes at $8''$ resolution [49], overlaid onto an image of the molecular CO(1-0) line emission [73]. **Right:** Polarized radio intensity (contours) and B-vectors of NCC 6946, combined from observations at 6 cm wavelength with the VLA and Effelsberg telescopes and smoothed to $15''$ resolution [7], overlaid onto an $H\alpha$ image from Anne Ferguson (Copyright: MPIfR Bonn; graphics: *Sterne und Weltraum*).

activity or by a small-scale dynamo [127].

In galaxies with massive *bars* the field lines follow the gas flow (Fig. 4 left). As the gas rotates faster than the bar pattern of a galaxy, a shock occurs in the cold gas that has a small sound speed, while the flow of warm, diffuse gas is only slightly compressed but sheared. The ordered field is also hardly compressed. It is probably coupled to the diffuse gas and strong enough to affect its flow [13]. The polarization pattern in barred galaxies can be used as a tracer of shearing gas flows in the sky plane and hence complements spectroscopic measurements of radial velocities.

The *central regions* of barred galaxies are often sites of ongoing intense star formation and strong magnetic fields that can affect the gas flow. NGC 1097 hosts a bright ring with about 1.5 kiloparsec diameter and an active nucleus in its center (Fig. 4 right). The ordered field in the ring has a spiral pattern and extends towards the nucleus. The orientation of the innermost spiral field agrees with that of the spiral dust filaments visible on optical images. Magnetic stress in the circumnuclear ring due to the strong total magnetic field (about $50 \mu\text{G}$) can drive gas inflow [4] at a rate of several M_{\odot}/yr , which is sufficient to fuel the activity of the nucleus [13].

Interaction with a dense intergalactic medium also imprints unique signatures onto magnetic fields and thus the radio emission. The Virgo cluster is a location of especially strong interaction effects (Fig. 5 left), and almost all cluster galaxies observed so far show asymmetries of their polarized emission because the outer magnetic fields were compressed by ram pressure or shearing gas flows [144, 145]. Ordered fields are an excellent tracer of past interactions between galaxies or with the intergalactic medium, or sweeping-up of the intracluster field [107].

Flocculent galaxies have disks but no prominent spiral arms. Nevertheless, spiral magnetic patterns exist in all flocculent galaxies observed so far, indicative that the

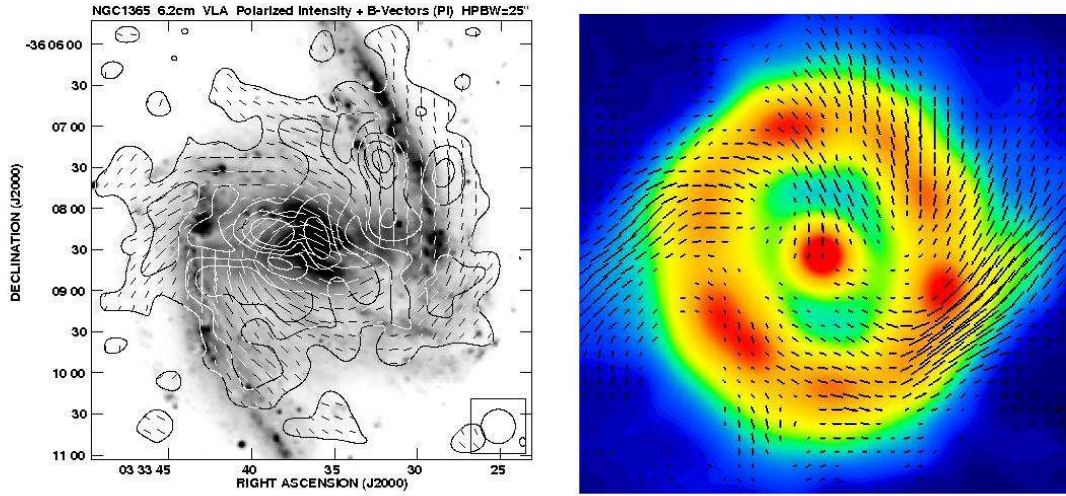


FIGURE 4. Left: Total radio intensity and B-vectors of the barred galaxy NGC 1365, observed at 6.2 cm wavelength with the VLA, smoothed to 25'' resolution and overlaid onto an optical image [13]. **Right:** Total radio intensity and B-vectors in the circumnuclear ring of the barred galaxy NGC 1097, observed at 3.5 cm wavelength with the VLA at 3'' resolution [13] (Copyright: MPIfR Bonn).

mean-field dynamo works independently of density waves. Ordered magnetic fields with strengths similar to those in grand-design spiral galaxies have been detected in the flocculent galaxies M 33 [132], NGC 3521 and NGC 5055 [78], and in NGC 4414 [122]. The mean degree of polarization (corrected for the differences in spatial resolution) is similar between grand-design and flocculent galaxies [78].

Radio continuum maps of *irregular*, slowly rotating galaxies may reveal strong total equipartition magnetic fields, e.g. in the Magellanic-type galaxy NGC 4449 where a fraction of the field is ordered with about $7 \mu\text{G}$ strength and a spiral pattern [30]. Faraday rotation shows that this ordered field is mostly regular and the mean-field dynamo is operating in this galaxy. Dwarf irregular galaxies with almost chaotic rotation do not have any regular fields and only spots of faint polarized emission [31]. The turbulent field strengths in starburst dwarfs are comparable to those in large spiral galaxies, e.g. in NGC 1569 [75], probably driven by a small-scale dynamo.

Nearby galaxies seen *edge-on* generally show a disk-parallel field near the disk plane [42]. As a result, polarized emission can also be detected from distant, unresolved galaxies if the inclination is larger than about 20° [126]. This opens a new method to search for ordered fields in distant galaxies. High-sensitivity radio polarization observations of edge-on galaxies like NGC 253 [71], NGC 891 [82] and NGC 5775 (Fig. 5 right) revealed vertical field components in the halo forming an X-shaped pattern which may be related to dynamo action [99] or outflows [38].

The stronger magnetic field in the central regions leads to larger synchrotron loss, leading to the “dumbbell” shape of many radio halos, e.g. in NGC 253 [70], which is in contrast to its almost spherical X-ray halo [106]. From the radio scale heights at several frequencies and the corresponding electron lifetimes (due to synchrotron, IC and adiabatic losses) a transport speed of about 300 km/s was measured for the halo of NGC 253 [70]. Similar radio scale heights of about 2 kpc of most edge-on galaxies

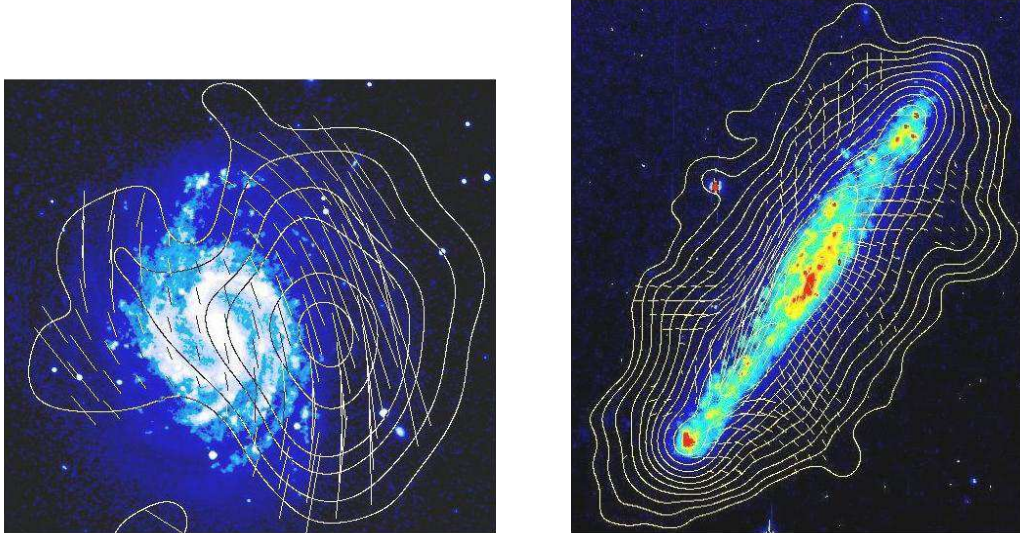


FIGURE 5. **Left:** Polarized radio intensity (contours) and B-vectors of the spiral galaxy NGC 4535 in the Virgo cluster, observed at 6.3 cm with the Effelsberg telescope [145]. The background optical image is from the Digital Sky Survey. **Right:** Total radio intensity and B-vectors of the edge-on galaxy NGC 5775, observed at 6.2 cm wavelength with the VLA at 17'' resolution [136].

TABLE 1. Typical field structures in galaxies

Galaxy type	Magnetic field structure	Regular field (dynamo)
Sc galaxy with strong density wave	Spiral field at inner edge and in interarm regions, turbulent field in arms	Weak or moderate
Sb or Sc galaxy with weak or moderate density wave	Spiral field in interarm regions, turbulent field in arms	Strong
Barred Sc galaxy	Ordered + turbulent field along bar, spiral field outside bar	Weak
Flocculent Sc or Sd galaxy	Spiral + turbulent field in disk	Weak
Irregular galaxy	Turbulent field in star-forming regions + segments of ordered field	Not detected
Starburst dwarf galaxy	Turbulent field in star-forming regions	Not detected
Spheroidal dwarf galaxy	Not detected	Not detected
Sa galaxy	Ordered + turbulent fields	Not detected
S0 galaxy	Not detected	Not detected
E galaxy (non-active nucleus)	Not detected	Not detected

observed so far, in spite of the different field strengths, indicates that the outflow speed increases with the average field strength and the star-formation rate [82].

In the exceptionally large radio halos around the irregular and interacting galaxies M 82 [113] and NGC 4631 [56] a few magnetic spurs could be resolved, connected to star-forming regions. These observations support the idea of a strong galactic outflow that is driven by regions of star formation in the inner disk.

Early-type galaxies (Sa, S0) and elliptical galaxies without an active nucleus have very little star formation and hence do not produce many cosmic rays emitting syn-

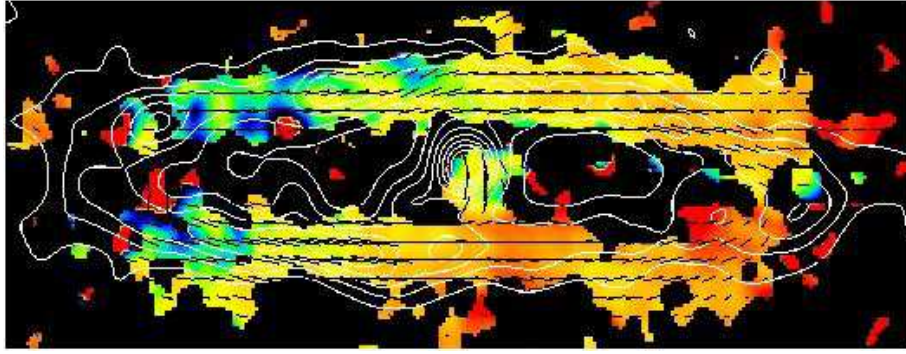


FIGURE 6. Total radio intensity (contours) and Faraday Rotation Measures (RM) in the Andromeda galaxy (M 31), determined from observations at 6 cm and 11 cm with the Effelsberg telescope [15]. The intrinsic RM varies between about -80 rad m^{-2} (left side of the major axis) and about $+80 \text{ rad m}^{-2}$ (right side of the major axis).

chrotron emission. The only deep observation of a Sa galaxy, M 104 with a prominent dust ring, revealed weak, ordered magnetic fields [85]. Large-scale regular magnetic fields may exist in differentially rotating galaxies even without any star formation because turbulence can be generated by the magneto-rotational instability (MRI) [119]. Their detection may become possible via RM grids of background sources with future radio telescopes.

FARADAY ROTATION AND DYNAMOS IN GALAXIES

Spiral magnetic patterns in galaxies can be generated by several mechanisms, like compression at the inner edge of spiral arms, by shear in interarm regions, or by dynamo action. For a distinction, *Faraday rotation measures* (RM) need to be measured from the diffuse polarized emission of the galaxy or from RM data of polarized background sources [125]. Large-scale RM patterns are a clear signature a mean-field dynamo. Several dynamo modes can be superimposed, so that a Fourier analysis is needed [81]. The resolution of present-day observations is sufficient to identify 2–3 modes.

The disks of about a dozen of nearby spiral galaxies reveal large-scale RM patterns. The Andromeda galaxy M 31 (Fig. 6) is the prototype of a dynamo-generated axisymmetric spiral disk field [47] which extends to 25 kpc distance from the center [62]. Other candidates for a dominating axisymmetric disk field (dynamo mode $m = 0$) are the nearby spiral IC 342 [83] and the irregular Large Magellanic Cloud (LMC) [54]. Dominating bisymmetric spiral fields (dynamo mode $m = 1$) are rare, with M 81 as the only known case [84]. Faraday rotation in the magnetic arms of NGC 6946 (Fig. 3 right) and in other similar galaxies can be described by a superposition of two azimuthal dynamo modes ($m = 0$ and $m = 2$) with about equal amplitudes where the quadrisymmetric spiral mode is phase shifted with respect to the density wave [7].

The spiral pattern of magnetic fields cannot be solely the result of mean-field dynamo action. If the beautiful spiral pattern of M 51 seen in radio polarization [49] were only due to a regular field, its line-of sight component should generate a conspicuous large-

scale pattern in Faraday rotation, which is not observed. This means that a large amount of the ordered field is *anisotropic* and probably generated by compression and shear of the non-axisymmetric gas flows in the density-wave potential. The anisotropic field is strongest at the positions of the prominent dust lanes on the inner edge of the inner gas spiral arms, due to compression of turbulent fields in the density-wave shock. A weak regular field (dynamo modes $m = 0$ and $m = 1$) also exists in the disk of M 51 [49].

In many other observed galaxy disks no clear patterns of Faraday rotation were found. Either several dynamo modes are superimposed and cannot be distinguished with the limited sensitivity and resolution of present-day telescopes, or the timescale for the generation of large-scale modes is longer than the galaxy's lifetime [3].

While the azimuthal symmetry of the magnetic field is known for many galaxies, the vertical symmetry (even or odd) is much harder to determine. The RM patterns of even and odd modes are similar in mildly inclined galaxies. The field of odd modes reverses its sign above and below the galactic plane. The symmetry type becomes only visible in strongly inclined galaxies, as the RM sign above and below the plane. Faraday RM data of NGC 253 indicate an even-symmetry field [71]. Indirect evidence for dominating even fields [20] comes from the asymmetry of polarized emission along the major axis observed at 1.4 GHz in many galaxies [69].

Large-scale field reversals at certain radial distances from a galaxy's center, like those in the Milky Way (see below), have not been detected in spiral galaxies so far, although high-resolution RM maps of Faraday rotation are available for many spiral galaxies. In the barred galaxy NGC 7479, where a jet serves as a bright polarized background and high-resolution observations were possible with high signal-to-noise ratio, several reversals on 1–2 kpc scale were detected in the foreground disk of the galaxy [92].

MAGNETIC FIELDS IN THE MILKY WAY

The detection of ultrahigh-energy cosmic rays (UHECRs) with the AUGER observatory and the anisotropic distribution of their arrival directions [1] calls for a proper model of particle propagation. As UHECR particles are deflected by large-scale regular fields and scattered by turbulent fields, the structure and extent of the fields in the disk and halo of the Milky Way need to be known.

Optical polarization data of about 5500 selected stars in the Milky Way yielded the orientation of the large-scale magnetic field near the sun [50], which is mostly parallel to the Galactic plane and oriented along the local spiral arm.

Surveys of the total synchrotron emission from the Milky Way yield equipartition strengths of the total field of $6 \mu\text{G}$ near the sun and about $10 \mu\text{G}$ in the inner Galaxy (Berkhuijsen, in [147]), consistent with Zeeman splitting data of low-density gas clouds [36]. In dense dust clouds field strengths of about $100 \mu\text{G}$ were measured from submillimeter polarimetry [35]. Zeeman splitting of OH maser lines from dense clouds yield field strengths of a few mG [46]. Milligauss fields were also found in pulsar wind nebulae from the break in the synchrotron spectrum [80].

In the nonthermal filaments near the Galactic Center the field strength is several $100 \mu\text{G}$ [45, 111, 152]. Their vertical orientation could be part of a poloidal field [45], which is hard to observe in external galaxies due to insufficient resolution. The break

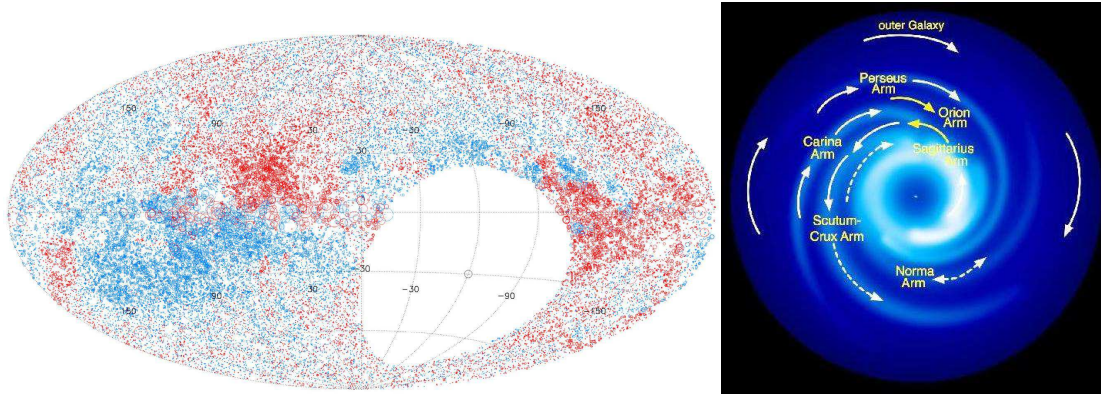


FIGURE 7. Left: All-sky map of rotation measures in the Milky Way, generated from the data of 37,543 polarized extragalactic sources from the VLA NVSS survey. Red circles: positive RM, blue circles: negative RM; the circle size scales with $|RM|$ [134]. **Right:** Model of the magnetic field in the Milky Way, derived from Faraday rotation measures of pulsars and extragalactic sources. Generally accepted results are indicated by yellow vectors, while white vectors are not fully confirmed (from Brown, priv. comm.).

in the synchrotron spectrum requires that the field near the Galactic Centre is at least $50 \mu\text{G}$ on 400 pc scale [34].

The all-sky maps of polarized synchrotron emission at 1.4 GHz from the Milky Way from DRAO and Villa Elisa and at 22.8 GHz from WMAP and the Effelsberg RM survey of polarized extragalactic sources were used to model the regular Galactic field [129, 130]. One large-scale *field reversal* is required at about 1–2 kpc from the sun towards the Milky Way’s center, which is also supported by pulsar RMs [51, 102] and RMs from extragalactic sources near the Galactic plane [137] (Fig. 7 right). More large-scale reversals may exist [63].

A satisfying explanation for the reversals in the Milky Way is still lacking. Nothing similar has been detected in external galaxies so far. The reversals may be restricted to a thin layer near to the plane and hence are hardly visible in the average RM data of external galaxies along the line of sight. Secondly, the reversals in the Milky Way may be of limited azimuthal extent, and then are difficult to observe in external galaxies with the resolution of present-day telescopes. Thirdly, the reversals in the Milky Way may be part of a disturbed field structure, e.g. due to interaction with the Magellanic clouds.

The signs of RMs of extragalactic sources and of pulsars at Galactic longitudes $l=90^\circ - 270^\circ$ are the same above and below the plane (Fig. 7 left): the local magnetic field is symmetric, while the RM signs towards the inner Galaxy ($l=270^\circ - 90^\circ$) are *opposite* above and below the plane. This can be assigned to an antisymmetric halo field [130] or to deviations of the local field [150]. In conclusion, the overall structure of the regular field in the disk of the Milky Way is not known yet [98, 103]. A larger sample of pulsar and extragalactic RM data is needed.

While the large-scale field is much more difficult to measure in the Milky Way than in external galaxies, Galactic observations can trace magnetic structures to much smaller scales [112]. Polarization surveys at 1.4 GHz [93, 149] and at lower frequencies [67, 118] reveal a wealth of structures on parsec and sub-parsec scales: filaments, canals, lenses and rings. They appear only in the maps of polarized intensity, but not in

total intensity. Some of these are artifacts due to strong depolarization of background emission in a foreground Faraday screen and carry valuable information about the turbulent ISM in the Faraday screen [48]. Other features are associated with real objects, like planetary nebulae [109] or the photodissociation regions of molecular clouds [148].

Little is known about the halo field in the Milky Way. The synchrotron scale height of about 1.5 kpc indicates a scale height of the total field of at least 6 kpc. The local regular Galactic field, according to RM data from extragalactic sources, has no significant vertical component towards the northern Galactic pole and only a weak vertical component of $B_z \simeq 0.3 \mu\text{G}$ towards the south [96].

GALAXY CLUSTERS

Some fraction of galaxy clusters, mostly the massive and X-ray bright ones, has diffuse radio emission [27], emerging from diffuse *halos* and steep-spectrum *relics* which can best be observed at low frequencies (Fig. 8). The diffuse halo emission is almost unpolarized and emerges from turbulent intracluster magnetic fields. RMs towards background sources show a vanishing mean value and a dispersion that decreases with distance from the cluster center [33]. Relics can emit highly polarized radio waves from anisotropic magnetic fields generated by compression in merger shocks [43, 59, 139]. The record-holder is a relic in a distant cluster of about 2 Mpc length and with a degree of polarization of 50–60% (Fig. 8 right).

The asymmetric polarized intensities of galaxies observed in the Virgo cluster [144, 145] (Fig. 5 left) can be interpreted as sweeping-up the intracluster magnetic field, if the galactic field is shielded, similar to the interaction between the solar wind and the Earth's magnetic field. The asymmetries may indicate that the intracluster field has a radial pattern, as predicted by the magneto-thermal instability [107]. In this case, future high-sensitivity observations should reveal weakly polarized emission from cluster halos.

Equipartition strengths of the total magnetic field range from 0.1 to 1 μG in halos [58], and are higher in relics. On the other hand, Faraday rotation data towards background sources behind cluster halos reveals fields of a few μG strength fluctuating on coherence scales of a few kpc [58] and even fields of 40 μG in the cores of cooling flow clusters [26] where they may be dynamically important. The reason for the difference in the field strength determinations is still under discussion.

High-resolution RM maps of radio galaxies embedded in a cluster allowed to derive the power spectra of the turbulent intracluster magnetic fields which are of Kolmogorov type [18, 142, 143].

INTERGALACTIC MAGNETIC FIELDS

Magnetic fields in the intergalactic medium (IGM) are of fundamental importance for cosmology [146]. Their role as the likely seed field for galaxies and clusters and their possible relation to structure formation in the early Universe place considerable importance on its discovery. Various generation mechanisms have been suggested. The field could be produced via the Weibel instability at structure formation shocks [97]. Another

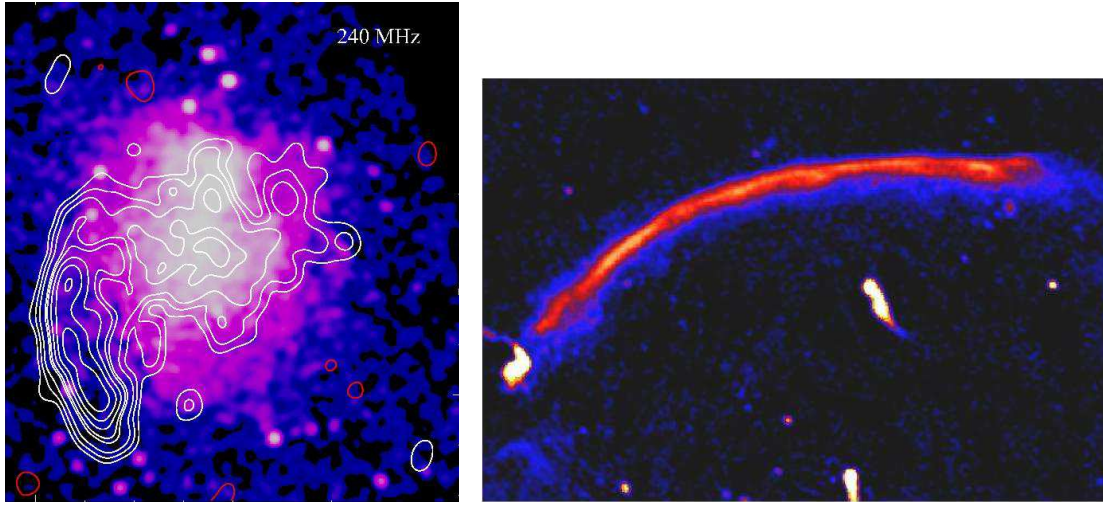


FIGURE 8. **Left:** Total radio intensity of the halo and relic (left edge) of the galaxy cluster Abell 521, observed at 240 MHz with the GMRT and smoothed to $35''$, overlaid onto an X-ray image from CHANDRA [23]. **Right:** Total radio intensity of the relic (the “sausage”) at the edge of the galaxy cluster CIZA J2242.8+5301 at a redshift of 0.1921, observed at 610 MHz with the GMRT at $4''$ resolution [139].

possibility is the injection from galactic black holes (AGNs) and outflows from starburst galaxies [141]. In each case the field is subsequently amplified by compression and large-scale shear flows [22]. Ryu et al. [115] have argued that highly efficient amplification is possible via MHD turbulence, with the source of the turbulent energy being the structure formation shocks themselves. Estimates of the strength of the turbulent field in filaments obtained from MHD simulations with a primordial seed field typically range between $0.1 \mu\text{G}$ and $0.01 \mu\text{G}$, while regular fields are weaker.

Until recently, there has been no unambiguous detection of a general magnetic field in the IGM. In an intergalactic region of about 2° extent west of the Coma Cluster, containing a group of radio galaxies, enhanced synchrotron emission may indicate an equipartition total field strength of $0.2 - 0.4 \mu\text{G}$ [89]. Xu et al. [151] observed an excess of rotation measures (RM) towards two super-clusters which may indicate regular magnetic fields of $< 0.3 \mu\text{G}$ on scales of order 500 kpc. Gamma-ray halos around active galactic nuclei can be used to measure the strength of the intergalactic field [2], but the observed halos could also be instrumental effects. Lee et al. [95] found indications for a statistical correlation at the 4σ level of the RMs of background sources with the galaxy density field which may correspond to an intergalactic field of about 30 nG strength and about 1 Mpc coherence length. However, the current data are probably insufficient to constrain the amplitude and distribution of large-scale intergalactic fields [124].

Progress came with the FERMI satellite. The non-observation of GeV γ -ray emission from the electromagnetic cascade in the IGM initiated by TeV γ -rays from blazars observed with HESS yields a *lower limit of the IGM magnetic field strength* of $3 \times 10^{-16} \text{ G}$ [101]. This IGM must be all-pervasive, with a filling factor of at least 60% [40].



FIGURE 9. LOFAR station in Tautenburg/Germany (Copyright: Michael Pluto, TLS).

PROSPECTS

Next-generation radio telescopes will widen the range of observable magnetic phenomena. At low frequencies, synchrotron emission can be observed from aging electrons far away from their places of origin. Low frequencies are also ideal to search for small Faraday rotation measures from weak interstellar and intergalactic fields [8] and in steep-spectrum cluster relics [23]. The recently completed *Low Frequency Array* (LOFAR) (Fig. 9), followed by the *Murchison Widefield Array* (MWA) and the *Long Wavelength Array* (LWA) (both under construction), are suitable instruments to search for weak magnetic fields in outer galaxy disks, galaxy halos and cluster halos.

LOFAR will detect all pulsars within 2 kpc of the sun and discover about 1000 new nearby pulsars, especially at high latitudes [138]. Most of these are expected to emit strong, linearly polarized signals at low frequencies. This will allow us to measure their RMs and to derive an unprecedented picture of the magnetic field near to the sun.

Deep high-resolution observations at high frequencies, where Faraday effects are small, require a major increase in sensitivity of continuum observations, to be achieved by the *Extended Very Large Array* (EVLA) and the planned *Square Kilometre Array* (SKA) [9] (Fig. 10). The detailed structure of the magnetic fields in the ISM of galaxies, in galaxy halos, cluster halos and cluster relics will be observed. The magnetic power spectra can be measured. Direct insight into the interaction between gas and magnetic fields in these objects will become possible. The SKA will also allow to measure the Zeeman effect of weak magnetic fields in the Milky Way and in nearby galaxies.

Detection of polarized emission from distant, unresolved galaxies will reveal large-scale ordered fields [126], to be compared with the predictions of dynamo theory [3]. The SKA at 1.4 GHz will detect Milky-Way type galaxies at $z \leq 1.5$ (Fig. 11 left) and their polarized emission at $z \leq 0.5$ (assuming 10% polarization). Bright starburst galaxies can be observed at larger redshifts, but are not expected to host ordered fields. Cluster relics are also detectable at large redshifts through their integrated polarized emission.

Unpolarized synchrotron emission, signature of turbulent magnetic fields, can be detected with the SKA in starburst galaxies out to large redshifts, depending on luminos-

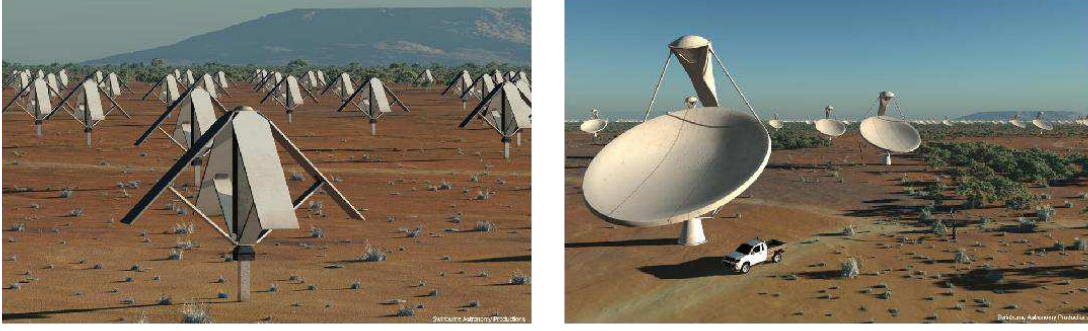


FIGURE 10. Planned SKA configurations: dipoles for low frequencies (70–450 MHz) (left) and dishes for high frequencies (450 MHz–3 GHz) (Copyright: Swinburne Astronomy Productions and SKA Project Development Office).

ity and magnetic field strength (Fig. 11 left), and for cluster halos. However, for fields weaker than $3.25 \mu\text{G} (1+z)^2$, energy loss of cosmic-ray electrons is dominated by the inverse Compton effect with CMB photons, so that the energy appears mostly in X-rays, not in the radio range. On the other hand, for strong fields the energy range of the electrons emitting at a 1.4 GHz drops to low energies, where ionization and bremsstrahlung losses become dominant [100]. In summary, the mere detection of synchrotron emission at high redshifts will constrain the range of allowed magnetic field strengths.

If polarized emission from galaxies, cluster halos or cluster relics is too weak to be detected, the method of *RM grids* towards background QSOs can still be applied and allows us to determine the field strength and pattern in an intervening galaxy. This method can be applied to distances of young QSOs ($z \simeq 5$). Regular fields of several μG strength were already detected in distant galaxies [16, 87, 90]. Mean-field dynamo theory predicts RMs from evolving regular fields with increasing coherence scale at $z \leq 3$ [3]. (Note that the observed RM values are reduced by the redshift dilution factor of $(1+z)^{-2}$.) A reliable model for the field structure of nearby galaxies, cluster halos and cluster relics needs RM values from a large number of polarized background sources, hence large sensitivity and/or high survey speed [86].

The *POSSUM* survey at 1.4 GHz with the *Australia SKA Pathfinder* (ASKAP) telescope (under construction) with 30 deg^2 field of view will measure about 100 RMs of extragalactic sources per square degree within 10 h integration time, about 100 times denser than in Fig. 7 (left). Similarly long integrations with the EVLA and with MeerKAT will show about 5 times more RMs, but their fields of view are smaller.

The *SKA Magnetism Key Science Project* plans to observe a wide-field survey (at least 10^4 deg^2) around 1 GHz with 1 h integration per field which will detect sources of $0.5 - 1 \mu\text{Jy}$ flux density and measure at least $1500 \text{ RMs deg}^{-2}$. This will contain at least $2 \cdot 10^7$ RMs from compact polarized extragalactic sources at a mean spacing of $\simeq 90''$ [53]. This survey will also be used to model the structure and strength of the magnetic fields in the Milky Way, in intervening galaxies and clusters and in the intergalactic medium [11]. The SKA pulsar survey will find about 20,000 new pulsars which will mostly be polarized and reveal RMs (Fig. 11 right), suited to map the Milky Way's magnetic field with high precision. More than 10,000 RM values are expected in the

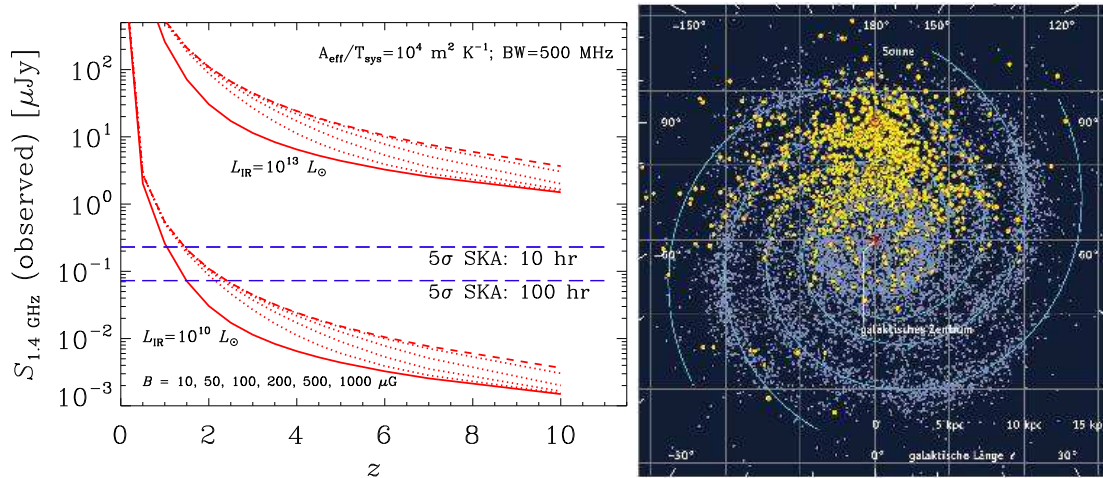


FIGURE 11. Left: Total synchrotron emission at 1.4 GHz as a function of redshift z and magnetic field strength B , and the 5σ detection limits for 10 h and 100 h integration time with the SKA [100]. **Right:** Simulation of about 20,000 pulsars (blue) in the Milky Way that will be detected with the SKA, compared to about 2000 pulsars known today (yellow). Graphics: *Sterne und Weltraum* (from Cordes, priv. comm).

area of M 31 and will allow the detailed reconstruction of the 3-D field structure. Simple patterns of regular fields can be recognized out to distances of about 100 Mpc [125] where the polarized flux is far too low to be mapped. The evolution of field strength in cluster halos can be measured by the RM grid to redshifts of about 1 [86].

If the filaments of the local Cosmic Web outside clusters contain a magnetic field [115], possibly enhanced by IGM shocks, we hope to detect this field by direct observation of its total synchrotron emission [76] and possibly its polarization, or by Faraday rotation towards background sources. For fields of $\approx 10^{-8} - 10^{-7}$ G with 1 Mpc coherence length and $n_e \approx 10^{-5} \text{ cm}^{-3}$ electron density, Faraday rotation measures between 0.1 and 1 rad m^{-2} are expected which will be hard to detect even with LOFAR. More promising is a statistical analysis like the measurement of the power spectrum of the magnetic field of the Cosmic Web [79] or the cross-correlation with other large-scale structure indicators like the galaxy density field [124].

If an overall IGM field with a coherence length of a few Mpc existed in the early Universe and its strength varied proportional to $(1+z)^2$, its signature may become evident at redshifts of $z > 3$. Averaging over a large number of RMs is required to unravel the IGM signal. The goal is to detect an IGM magnetic field of 0.1 nG, which needs an RM density of $\approx 1000 \text{ sources deg}^{-2}$ [79], achievable with the SKA. Detection of a general IGM field, or placing stringent upper limits on it, will provide powerful observational constraints on the origin of cosmic magnetism.

REFERENCES

1. P. Abreu, and The Pierre Auger Collaboration, *Astroparticle Phys.* **34**, 314–326 (2010).
2. S. Ando, and A. Kusenko, *ApJ* **722**, L39–L44 (2010).
3. T. G. Arshakian, R. Beck, M. Krause, and D. Sokoloff, *A&A* **494**, 21–32 (2009).

4. S. A. Balbus, and J. F. Hawley, *Rev. Mod. Phys.* **70**, 1–53 (1998).
5. S. A. Balbus, and C. S. Reynolds, *ApJ* **681**, L65–L68 (2008).
6. R. Beck, in *Cosmic Magnetic Fields*, eds. R. Wielebinski and R. Beck, Springer, Berlin, 2005, pp. 41–68.
7. R. Beck, *A&A* **470**, 539–556 (2007).
8. R. Beck, *Rev. Mex. AyA* **36**, 1–8 (2009).
9. R. Beck, http://www.scholarpedia.org/article/Square_kilometre_array (2010).
10. R. Beck, A. Brandenburg, D. Moss, A. Shukurov, and D. Sokoloff, *Ann. Rev. A&A* **34**, 155–206 (1996).
11. R. Beck, and B. M. Gaensler, in *Science with the Square Kilometer Array*, eds. C. Carilli and S. Rawlings, *New Astr. Rev.* **48**, Elsevier, Amsterdam, 2004, pp. 1289–1304.
12. R. Beck, and M. Krause, *Astron. Nachr.* **326**, 414–427 (2005).
13. R. Beck, A. Fletcher, A. Shukurov, et al., *A&A* **444**, 739–765 (2005).
14. E. F. Bell, *ApJ* **586**, 794–813 (2003).
15. E. M. Berkhuijsen, R. Beck, and P. Hoernes, *A&A* **398**, 937–948 (2003).
16. M. L. Bernet, F. Miniati, S. J. Lilly, P. P. Kronberg, and M. Dessauges-Zavadsky, *Nature* **454**, 302–304 (2008).
17. S. Bertone, C. Vogt, and T. A. Enßlin, *MNRAS* **370**, 319–330 (2006).
18. A. Bonafede, L. Feretti, M. Murgia, et al., *A&A* **513**:A30 (2010).
19. A. Brandenburg, and K. Subramanian, *Phys. Rep.* **417**, 1–209 (2005).
20. R. Braun, G. Heald, and R. Beck, *A&A* **514**:A42 (2010).
21. M. A. Brentjens, and A. G. de Bruyn, *A&A* **441**, 1217–1228 (2005).
22. M. Brüggen, M. Ruszkowski, A. Simionescu, M. Hoeft, and C. Dalla Vecchia, *ApJ* **631**, L21–L24 (2005).
23. G. Brunetti, S. Giacintucci, R. Cassano, et al., *Nature* **455**, 944–947 (2008).
24. B. J. Burn, *MNRAS* **133**, 67–83 (1966).
25. C. Caprini, R. Durrer, and E. Fenu, *J. Cosmology & Astroparticle Phys.* **11**:001 (2009).
26. C. L. Carilli, and G. B. Taylor, *Ann. Rev. A&A* **40**, 319–348 (2002).
27. R. Cassano, G. Brunetti, T. Venturi, et al., *A&A* **480**, 687–697 (2008).
28. K. T. Chyży, *A&A* **482**, 755–769 (2008).
29. K. T. Chyży, and R. J. Buta, *ApJ* **677**, L17–L20 (2008).
30. K. T. Chyży, R. Beck, S. Kohle, U. Klein, and M. Urbanik, *A&A* **355**, 128–137 (2000).
31. K. T. Chyży, J. Knapik, D. J. Bomans, et al., *A&A* **405**, 513–524 (2003).
32. K. T. Chyży, and R. Beck, *A&A* **417**, 541–555 (2004).
33. T. E. Clarke, P. P. Kronberg, and H. Böhringer, *ApJ* **547**, L111–L114 (2001).
34. R. M. Crocker, D. I. Jones, F. Melia, J. Ott, and R. J. Protheroe, *Nature* **463**, 65–67 (2010).
35. R. M. Crutcher, D. J. Nutter, D. Ward-Thompson, and J. M. Kirk, *ApJ* **600**, 279–285 (2004).
36. R. M. Crutcher, B. Wandelt, C. Heiles, E. Falgarone, and T. H. Troland, *ApJ* **725**, 466–479 (2010).
37. M. A. de Avillez, and D. Breitschwerdt, *A&A* **436**, 585–600 (2005).
38. C. Dalla Vecchia, and J. Schaye, *MNRAS* **387**, 1431–1444 (2008).
39. C. L. Dobbs, and D. J. Price, *MNRAS* **383**, 497–512 (2008).
40. K. Dolag, M. Kachelriess, S. Ostapchenko, and R. Tomas, *ApJ* **727**:L4 (2011).
41. G. Dumas, E. Schinnerer, F. S. Tabatabaei, et al., *AJ* **141**:41 (2011).
42. M. Dumke, M. Krause, R. Wielebinski, and U. Klein, *A&A* **302**, 691–703 (1995).
43. T. A. Enßlin, P. L. Biermann, U. Klein, and S. Kohle, *A&A* **332**, 395–409 (1998).
44. K. Ferrière, and D. Schmitt, *A&A* **358**, 125–143 (2000).
45. K. Ferrière, *A&A* **505**, 1183–1198 (2009).
46. V. L. Fish, M. J. Reid, A. L. Argon, and K. M. Menten, *ApJ* **596**, 328–343 (2003).
47. A. Fletcher, E. M. Berkhuijsen, R. Beck, and A. Shukurov, *A&A* **414**, 53–67 (2004).
48. A. Fletcher, and A. Shukurov, *MNRAS* **371**, L21–L25 (2006).
49. A. Fletcher, R. Beck, A. Shukurov, E. M. Berkhuijsen, and C. Horellou, *MNRAS* **412**, 2396–2416 (2011).
50. P. Fosalba, A. Lazarian, S. Prunet, and J. A. Tauber, *ApJ* **546**, 762–772 (2002).
51. P. Frick, R. Stepanov, A. Shukurov, and D. Sokoloff, *MNRAS* **325**, 649–664 (2001).
52. P. Frick, D. Sokoloff, R. Stepanov, and R. Beck, *MNRAS*, in press, arXiv:1102.4316 (2011).

53. B. M. Gaensler, R. Beck, and L. Feretti, in *Science with the Square Kilometer Array*, eds. C. Carilli and S. Rawlings, *New Astr. Rev.* **48**, Elsevier, Amsterdam, 2004, pp. 1003–1012.
54. B. M. Gaensler, M. Haverkorn, L. Staveley-Smith, et al., *Science* **307**, 1610–1612 (2005).
55. C. Gissinger, S. Fromang, and E. Dormy, *MNRAS* **394**, L84–L88 (2009).
56. G. Golla, and E. Hummel, *A&A* **284**, 777–792 (1994).
57. G. C. Gómez, and D. P. Cox, *ApJ* **580**, 235–252 (2002).
58. F. Govoni, and L. Feretti, *Int. J. Mod. Phys. D* **13**, 1549–1594 (2004).
59. F. Govoni, M. Murgia, L. Feretti, et al., *A&A* **430**, L5–L8 (2005).
60. J. S. Greaves, W. S. Holland, T. Jenness, and T. G. Hawarden, *Nature* **404**, 732–733 (2000).
61. O. Gressel, D. Elstner, U. Ziegler, and G. Rüdiger, *A&A* **486**, L35–L38 (2008).
62. J. L. Han, R. Beck, and E. M. Berkhuijsen, *A&A* **335**, 1117–1123 (1998).
63. J. L. Han, R. N. Manchester, A. G. Lyne, G. J. Qiao, and W. van Straten, *ApJ* **642**, 868–881 (2006).
64. M. Hanasz, K. Otmianowska-Mazur, and H. Lesch, *A&A* **386**, 347–358 (2002).
65. M. Hanasz, D. Wółtański, and K. Kowalik, *ApJ* **706**, L155–L158 (2009).
66. H. Hanayama, K. Takahashi, K. Kotake, et al., *ApJ* **633**, 941–945 (2005).
67. M. Haverkorn, P. Katgert, and A. G. de Bruyn, *A&A* **427**, 549–559 (2004).
68. G. Heald, in *Cosmic Magnetic Fields: From Planets, to Stars and Galaxies*, eds. K. G. Strassmeier, A. G. Kosovichev and J. E. Beckman, Cambridge Univ. Press, Cambridge, 2009, pp. 591–600.
69. G. Heald, R. Braun, and R. Edmonds, *A&A* **503**, 409–435 (2009).
70. V. Heesen, R. Beck, M. Krause, and R.-J. Dettmar, *A&A* **494**, 563–577 (2009).
71. V. Heesen, M. Krause, R. Beck, and R.-J. Dettmar, *A&A* **506**, 1123–1135 (2009).
72. F. Heitsch, E. G. Zweibel, A. D. Slyz, and J. E. G. Devriendt, *ApJ* **603**, 165–179 (2004).
73. T. T. Helfer, M. D. Thornley, M. W. Regan, et al., *ApJS* **145**, 259–327 (2003).
74. A. Hughes, T. Wong, R. Ekers, et al., *MNRAS* **370**, 363–379 (2006).
75. A. A. Kepley, S. Mühle, J. Everett, et al., *ApJ* **712**, 536–557 (2010).
76. U. Keshet, E. Waxman, and A. Loeb, in *Science with the Square Kilometer Array*, eds. C. Carilli and S. Rawlings, *New Astr. Rev.* **48**, Elsevier, Amsterdam, 2004, pp. 1119–1135.
77. U. Klein, R. Wielebinski, and H. W. Morsi, *A&A* **190**, 41–46 (1988).
78. J. Knapik, M. Soida, R.-J. Dettmar, R. Beck, and M. Urbanik, *A&A* **362**, 910–920 (2000).
79. T. Kolatt, *ApJ* **495**, 564–579 (1998).
80. R. Kothes, T. L. Landecker, W. Reich, S. Safi-Harb, and Z. Arzoumanian, *ApJ* **687**, 516–531 (2008).
81. M. Krause, in *Galactic and Intergalactic Magnetic Fields*, eds. R. Beck, R. Wielebinski, and P. P. Kronberg, Kluwer, Dordrecht, 1990, pp. 187–196.
82. M. Krause, *Rev. Mex. AyA* **36**, 25–29 (2009).
83. M. Krause, E. Hummel, and R. Beck, *A&A* **217**, 4–16 (1989).
84. M. Krause, R. Beck, and E. Hummel, *A&A* **217**, 17–30 (1989).
85. M. Krause, R. Wielebinski, and M. Dumke, *A&A* **448**, 133–142 (2006).
86. M. Krause, P. Alexander, R. Bolton, J. Geisbüsch, D. A. Green, and J. Riley, *MNRAS* **400**, 646–656 (2009).
87. P. P. Kronberg, J. J. Perry, and E. L. H. Zukowski, *ApJ* **387**, 528–535 (1992).
88. P. P. Kronberg, H. Lesch, and U. Hopp, *ApJ* **511**, 56–64 (1999).
89. P. P. Kronberg, R. Kothes, C. J. Salter, and P. Perillat, *ApJ* **659**, 267–274 (2007).
90. P. P. Kronberg, M. L. Bernet, F. Miniati, S. J. Lilly, M. B. Short, and D. M. Higdon, *ApJ* **676**, 70–79 (2008).
91. B. C. Lacki, T. A. Thompson, E. Quataert, *ApJ* **717**, 1–28 (2010).
92. S. Laine, and R. Beck, *ApJ* **673**, 128–142 (2008).
93. T. L. Landecker, W. Reich, R. I. Reid, et al., *A&A* **520**, A80 (2010).
94. M. Lazar, R. Schlickeiser, R. Wielebinski, S. Poedts, *ApJ* **693**, 1133–1141 (2009).
95. J. Lee, U.-L. Pen, A. R. Taylor, J. M. Stil, and C. Sunstrum, arXiv:0906.1631 (2009).
96. S. A. Mao, B. M. Gaensler, M. Haverkorn, et al., *ApJ* **714**, 1170–1186 (2010).
97. M. V. Medvedev, L. O. Silva, M. Fiore, R. A. Fonseca, and W. B. Mori, *JKAS* **37**, 533–541 (2004).
98. H. Men, K. Ferrière, and J. L. Han, *A&A* **486**, 819–828 (2008).
99. D. Moss, D. Sokoloff, R. Beck, and M. Krause, *A&A* **512**:A61 (2010).
100. E. Murphy, *ApJ* **706**, 482–496 (2009).
101. A. Neronov, and I. Vovk, *Science* **328**, 73–75 (2010).
102. T. Nota, and P. Katgert, *A&A* **513**:A65 (2010).

103. A. Noutsos, in *Cosmic Magnetic Fields: From Planets, to Stars and Galaxies*, eds. K. G. Strassmeier et al., Cambridge Univ. Press, Cambridge, 2009, pp. 15–24.
104. N. Oppermann, H. Junklewitz, G. Robbers, and T. A. Enßlin, *A&A*, in press, arXiv:1008.1264 (2010).
105. I. J. Parrish, and E. Quataert, *ApJ* **677**, L9–L12 (2008).
106. W. Pietsch, A. Vogler, U. Klein, and H. Zinnecker, *A&A* **360**, 24–48 (2000).
107. C. Frommer, and J. L. Dursi, *Nature Phys.* **6**, 520–526 (2010).
108. D. J. Price, and M. R. Bate, *MNRAS* **385**, 1820–1834 (2008).
109. R. R. Ransom, B. Uyaniker, R. Kothes, and T. L. Landecker, *ApJ* **684**, 1009–1017 (2008).
110. M. J. Rees, in *Cosmic Magnetic Fields*, eds. R. Wiełebinski and R. Beck, Springer, Berlin, 2005, pp. 1–8.
111. W. Reich, in *The Nuclei of Normal Galaxies*, eds. R. Genzel and A. I. Harris, Kluwer, Dordrecht, 1994, pp. 55–62.
112. W. Reich, in *Cosmic Polarization*, ed. R. Fabbri, Research Signpost, Kerala, 2006, pp. 91–130.
113. H.-P. Reuter, U. Klein, H. Lesch, R. Wiełebinski, and P. P. Kronberg, *A&A* **282**, 724–730 (1994).
114. T. Robshaw, E. Quataert, and C. Heiles, *ApJ* **680**, 981–998 (2008).
115. D. Ryu, H. Kang, J. Cho, and S. Das, *Science* **320**, 909–912 (2008).
116. S. M. Scarrott, D. Ward-Thompson, and R. F. Warren-Smith, *MNRAS* **224**, 299–305 (1987).
117. D. R. G. Schleicher, R. Banerjee, S. Sur, et al., *A&A* **522**:A115 (2010).
118. D. H. F. M. Schnitzeler, P. Katgert, and A. G. de Bruyn, *A&A* **494**, 611–622 (2009).
119. J. A. Sellwood, and S. A. Balbus, *ApJ* **511**, 660–665 (1999).
120. N. Seymour, T. Dwelly, D. Moss, et al., *MNRAS* **386**, 1695–1708 (2008).
121. A. Shukurov, D. Sokoloff, K. Subramanian, and A. Brandenburg, *A&A* **448**, L33–L36 (2006).
122. M. Soida, R. Beck, M. Urbanik, M., and J. Braine, *A&A* **394**, 47–57 (2002).
123. D. D. Sokoloff, A. A. Bykov, A. Shukurov, E. M. Berkhuijsen, R. Beck, and A. D. Poezd, *MNRAS* **299**, 189–206 (1998) and Erratum in *MNRAS* **303**, 207–208 (1999).
124. F. Stasyszyn, S. E. Nuza, K. Dolag, R. Beck, and J. Donnert, *MNRAS* **408**, 684–694 (2010).
125. R. Stepanov, T. G. Arshakian, R. Beck, P. Frick, and M. Krause, *A&A* **480**, 45–59 (2008).
126. J. M. Stil, M. Krause, R. Beck, A. R. Taylor, *ApJ* **693**, 1392–1403 (2009).
127. K. Subramanian, *MNRAS* **294**, 718–728 (1998).
128. K. Subramanian, A. Shukurov, and N. E. L. Haugen, *MNRAS* **366**, 1437–1454 (2006).
129. X. H. Sun, W. Reich, A. Waelkens, and T. A. Enßlin, *A&A* **477**, 573–592 (2008).
130. X. H. Sun, and W. Reich, *Research in A&A* **10**, 1287–1297 (2010).
131. F. Tabatabaei, R. Beck, M. Krause, et al., *A&A* **466**, 509–519 (2007).
132. F. Tabatabaei, M. Krause, A. Fletcher, and R. Beck, *A&A* **490**, 1005–1017 (2008).
133. J.-W. Tang, P. T. P. Ho, P. M. Koch, et al., *ApJ* **700**, 251–261 (2009).
134. A. R. Taylor, J. M. Stil, and C. Sunstrum, *ApJ* **702**, 1230–1236 (2009).
135. T. A. Thompson, E. Quataert, E. Waxman, N. Murray, and C. L. Martin, *ApJ* **645**, 186–198 (2006).
136. R. Tüllmann, R.-J. Dettmar, M. Soida, M. Urbanik, and J. Rossa, *A&A* **364**, L36–L41 (2000).
137. C. L. Van Eck, J. C. Brown, J. M. Stil, et al., *ApJ* **728**:97 (2011).
138. J. van Leeuwen, and B. W. Stappers, *A&A* **509**:A7 (2010).
139. R. J. van Weeren, H. J. A. Röttgering, M. Brüggen, and M. Hoeft, *Science* **330**, 347–349 (2010).
140. E. Vázquez-Semadeni, J. Kim, and J. Ballesteros-Paredes, *ApJ* **630**, L49–L52 (2005).
141. H. J. Völk, and A. M. Atoyan, *ApJ* **541**, 88–94 (2000).
142. C. Vogt, and T. A. Enßlin, *A&A* **412**, 373–385 (2003).
143. C. Vogt, and T. A. Enßlin, *A&A* **434**, 67–76 (2005).
144. B. Vollmer, M. Soida, R. Beck, et al., *A&A* **464**, L37–L40 (2007).
145. M. Weżgowiec, M. Urbanik, B. Vollmer, et al., *A&A* **471**, 93–102 (2007).
146. L. M. Widrow, *Rev. Mod. Phys.* **74**, 775–823 (2002).
147. R. Wiełebinski, in *Cosmic Magnetic Fields*, eds. R. Wiełebinski and R. Beck, Springer, Berlin, 2005, pp. 89–112.
148. M. Wolleben, and W. Reich, *A&A* **427**, 537–548 (2004).
149. M. Wolleben, T. L. Landecker, W. Reich, and R. Wiełebinski, *A&A* **448**, 411–424 (2006).
150. M. Wolleben, A. Fletcher, T. L. Landecker, et al., 2010, *ApJ* **724**, L48–L52 (2010).
151. Y. Xu, P. P. Kronberg, S. Habib, and Q. W. Dufton, *ApJ* **637**, 19–26 (2006).
152. F. Yusef-Zadeh, D. A. Roberts, W. M. Goss, D. A. Frail, and A. J. Green, *ApJ* **466**, L25–L29 (1996).